Phononic crystals of poroelastic spheres

A. Alevizaki, R. Sainidou, P. Rembert, B. Morvan, N. Stefanou

Phononic crystals of poroelastic spheres

A. Alevizaki,[1,2] R. Sainidou,[1,*] P. Rembert,[1] B. Morvan,[1] and N. Stefanou[2]

[1]*Normandie Université, UNIHAVRE, Laboratoire Ondes et Milieux Complexes, UMR CNRS 6294, 75 rue Bellot, 76600 Le Havre, France*

[2]*Department of Solid State Physics, National and Kapodistrian University of Athens, University Campus, GR-157 84 Athens, Greece*

(Received 19 July 2016; revised manuscript received 28 September 2016; published 23 November 2016)

An extension of the layer-multiple-scattering method to phononic crystals of poroelastic spheres immersed in a fluid medium is developed. The applicability of the method is demonstrated on specific examples of close-packed fcc crystals of submerged water-saturated meso- and macroporous silica microspheres. It is shown that, by varying the pore size and/or the porosity, the transmission, reflection, and absorption spectra of finite slabs of these crystals are significantly altered. Strong absorption, driven by the slow waves in the poroelastic material and enhanced by multiple scattering, leads to negligible transmittance over an extended frequency range, which might be useful for practical applications in broadband acoustic shielding. The results are analyzed by reference to relevant phononic dispersion diagrams in the viscous and inertial coupling limits, and a consistent interpretation of the underlying physics is provided.

DOI: 10.1103/PhysRevB.94.174306

I. INTRODUCTION

Phononic crystals are composite materials with elastic coefficients (mass density and elastic moduli or, equivalently, mass density and elastic wave velocities) that vary periodically in space [1,2]. In three dimensions they can be realized, e.g., by a periodic arrangement of solid or fluid inclusions in an otherwise homogeneous host medium (solid or fluid) of different elastic coefficients, although various other phononic architectures have also been considered in one and two dimensions. A most interesting aspect of these materials arises from the possibility of frequency regions, known as phononic band gaps, over which there can be no propagation of elastic waves in the crystal [3–5], but appropriately designed periodic or aperiodic phononic structures can exhibit a plethora of other interesting physical phenomena, including filtering [6], waveguiding [7–9], sensing [10], negative refraction, and focusing [11], with most of these properties usually occurring at wavelengths commensurate with the size of the unit cell. Nowadays, modern self-assembly and other nanofabrication techniques allow for the realization of hypersonic phononic crystals operating in the gigahertz range, with an example being colloidal crystals of silica nanospheres in a waterlike liquid. At these frequencies, however, Brillouin light-scattering experiments provide evidence that porosity in the silica particles cannot be neglected [12–14].

The acoustic properties of poroelastic materials at different length scales, such as rocks, soil, polymer networks, colloidal particles, and biological tissues, attract considerable interest from different scientific communities, ranging from geophysics to chemistry, materials physics, and biomedical sciences [15–17]. Phononic crystals comprising poroelastic materials offer the possibility of additional degrees of freedom, e.g., porosity, pore size, and fluid viscosity, to control the propagation of elastic waves and could exhibit unprecedented properties. However, to the best of our knowledge, apart from one-dimensional layered structures [18], phononic crystals of poroelastic inclusions in a fluid host medium have not been considered so far.

In the present paper we develop an extension of the layer-multiple-scattering method [19,20] to phononic crystals of poroelastic spheres immersed in a fluid medium. In Sec. II we briefly survey Biot's theory [21–24] for poroelastic materials. In Sec. III we provide explicit expressions for the scattering transition T matrix of a submerged fluid-saturated poroelastic sphere in the specific basis of vector spherical waves employed in our formalism. This matrix is the necessary ingredient in the development of the layer-multiple-scattering method for phononic crystals of poroelastic spheres that we describe in Sec. IV. In the same section we demonstrate the applicability of the method with specific examples of close-packed fcc crystals of meso- and macroporous silica microspheres immersed in water. In the last section we summarize the main findings of our paper.

II. ACOUSTIC WAVES IN POROELASTIC MATERIALS

In the framework of Biot's theory [21–24], a fluid-saturated poroelastic material is considered a macroscopically homogeneous and isotropic two-component (solid-fluid) system, which can be described in terms of average parameters. Its skeletal frame is made of a solid material, characterized by mass density ρ_s, bulk modulus K_s, and shear modulus (Lamé constant) μ_s in its consolidated compact form, while the bare skeletal frame has different elastic moduli, K_b and μ_b. The fluid, of mass density ρ_f and bulk modulus K_f, fills the whole volume of interconnected pores. It should be noted that sealed pore space is considered part of the solid frame and the (effective) porosity f is defined as the volume fraction occupied by the fluid. Denoting the average macroscopic displacement fields of the solid frame and the saturating fluid in space-time $(\mathbf{r},t)$ by $\mathbf{u}$ and $\mathbf{U}$, respectively, the corresponding effective stress tensors are given by

$$\begin{aligned}\overleftrightarrow{T} &= \mu_b \overleftrightarrow{I} \times \nabla \times \mathbf{u} + 2\mu_b \nabla \mathbf{u} \\ &\quad + \overleftrightarrow{I}(P - 2\mu_b)\nabla \cdot \mathbf{u} + \overleftrightarrow{I} Q \nabla \cdot \mathbf{U}, \\ \overleftrightarrow{S} &= \overleftrightarrow{I} Q \nabla \cdot \mathbf{u} + \overleftrightarrow{I} R \nabla \cdot \mathbf{U}, \end{aligned} \tag{1}$$

*sainidor@univ-lehavre.fr

where

$$P = K_s \frac{(1-f)(1-f-K_b/K_s)+fK_b/K_f}{1-f-K_b/K_s+fK_s/K_f} + \frac{4\mu_b}{3},$$
$$Q = \frac{fK_s(1-f-K_b/K_s)}{1-f-K_b/K_s+fK_s/K_f}, \quad (2)$$
$$R = \frac{f^2K_s}{1-f-K_b/K_s+fK_s/K_f}.$$

The macroscopic stress tensor $\overleftrightarrow{\sigma}$ and the mean pore fluid pressure p are given by

$$\overleftrightarrow{\sigma} = \overleftrightarrow{T} + \overleftrightarrow{S} \quad (3)$$

and

$$\overleftrightarrow{S} = -\overleftrightarrow{I}\, fp, \quad (4)$$

respectively.

Elastic wave propagation in this medium is governed by the following equations:

$$\rho_{11}\ddot{\mathbf{u}} + \rho_{12}\ddot{\mathbf{U}} + b(\dot{\mathbf{u}} - \dot{\mathbf{U}}) = \nabla \cdot \overleftrightarrow{T},$$
$$\rho_{12}\ddot{\mathbf{u}} + \rho_{22}\ddot{\mathbf{U}} - b(\dot{\mathbf{u}} - \dot{\mathbf{U}}) = \nabla \cdot \overleftrightarrow{S}, \quad (5)$$

where the overdot denotes the partial time derivative and

$$\rho_{11} = (1-f)\rho_s + (\alpha-1)f\rho_f,$$
$$\rho_{12} = -(\alpha-1)f\rho_f, \quad (6)$$
$$\rho_{22} = \alpha f\rho_f,$$

with α ($\alpha > 1$), the so-called tortuosity of the medium, being an intrinsic geometrical property related to variations in pore shapes and orientations [24–26]. The last term on the left-hand sides of Eqs. (5) accounts for frictional dissipation associated with relative motion between the fluid and solid components of the medium, where b is a damping coefficient. Intrinsic absorption of the solid frame and the infiltrated fluid can be taken into account by considering complex elastic constants.

At low frequencies, assuming that the flow of the fluid relative to the solid through the pores is of the Poiseuille type, the coefficient b is related to Darcy's coefficient of permeability κ_D by $b = f^2\eta/\kappa_D$, where η is the fluid viscosity [21]. The assumption of Poiseuille flow breaks down at high frequencies, and b can be written in a general form, which encompasses both the low- and high-frequency ranges, as follows [22]:

$$b = \frac{f^2\eta}{\kappa_D} \frac{i\zeta^2 J_0'(\sqrt{i}\zeta)}{4\sqrt{i}\zeta J_0(\sqrt{i}\zeta) + 8J_0'(\sqrt{i}\zeta)}, \quad (7)$$

where J_0 is the zero-order Bessel function of the first kind [27] and the prime denotes the first derivative with respect to the argument of the function. In the simple case of cylindrical pores parallel to the direction of the flow, $\zeta = R_p\sqrt{\omega\rho_f/\eta}$, where R_p is the radius of the cylinder [22]. In the general case, R_p can be considered a characteristic pore-size parameter that takes into account the geometry of the pores. The expression that multiplies the factor $f^2\eta/\kappa_D$ on the right-hand side of Eq. (7), considered a function of the real dimensionless variable ζ, over the entire range $0 \leqslant \zeta < \infty$ behaves similarly to the simple function $\sqrt{1-i(\zeta/4)^2}$, with their absolute relative difference being always less than 10%. Moreover, the geometrical parameters f, α, κ_D, R_p, which characterize the pores and are, in general, unrelated, for a set of nonintersecting canted cylindrical pores are related to each other by the equation $fR_p^2 = 8\alpha\kappa_D$, which leads to the following simple yet effective form for b [28]:

$$b = \frac{f^2\eta}{\kappa_D}\left(1 - i\frac{\alpha\kappa_D\rho_f\omega}{2f\eta}\right)^{1/2}. \quad (8)$$

We assume monochromatic time-harmonic solutions of Eqs. (5), of angular frequency ω, in the forms $\mathbf{u}(\mathbf{r},t) = \mathrm{Re}[\mathbf{u}(\mathbf{r})\exp(-i\omega t)]$ and $\mathbf{U}(\mathbf{r},t) = \mathrm{Re}[\mathbf{U}(\mathbf{r})\exp(-i\omega t)]$. Decomposing the general displacement fields into longitudinal (irrotational) and transverse (divergenceless) vector components, denoted by a subscript l and t, respectively, Eqs. (1) and (5) lead to two separate systems of linear equations. For the longitudinal modes we obtain

$$P\nabla[\nabla\cdot\mathbf{u}_l(\mathbf{r})] + Q\nabla[\nabla\cdot\mathbf{U}_l(\mathbf{r})] + \widetilde{\rho}_{11}\omega^2\mathbf{u}_l(\mathbf{r}) + \widetilde{\rho}_{12}\omega^2\mathbf{U}_l(\mathbf{r}) = 0,$$
$$Q\nabla[\nabla\cdot\mathbf{u}_l(\mathbf{r})] + R\nabla[\nabla\cdot\mathbf{U}_l(\mathbf{r})] + \widetilde{\rho}_{12}\omega^2\mathbf{u}_l(\mathbf{r}) + \widetilde{\rho}_{22}\omega^2\mathbf{U}_l(\mathbf{r}) = 0, \quad (9)$$

where $\widetilde{\rho}_{11} = \rho_{11} + ib/\omega$, $\widetilde{\rho}_{12} = \rho_{12} - ib/\omega$, and $\widetilde{\rho}_{22} = \rho_{22} + ib/\omega$. Equations (9) accept plane-wave solutions of the forms $\mathbf{u}_l(\mathbf{r}) = \mathbf{u}_{l0}\exp(i\mathbf{q}\cdot\mathbf{r})$ and $\mathbf{U}_l(\mathbf{r}) = \mathbf{U}_{l0}\exp(i\mathbf{q}\cdot\mathbf{r})$, where the wave number q satisfies the biquadratic equation

$$(PR-Q^2)q^4 - (\widetilde{\rho}_{11}R + \widetilde{\rho}_{22}P - 2\widetilde{\rho}_{12}Q)\omega^2q^2 + (\widetilde{\rho}_{11}\widetilde{\rho}_{22} - \widetilde{\rho}_{12}^2)\omega^4 = 0. \quad (10)$$

The two positive roots of Eq. (10), q_1 and q_2, which are physically acceptable, correspond to the so-called fast and slow longitudinal waves, respectively. The corresponding displacement fields are related through $\mathbf{U}_\nu = A_\nu\mathbf{u}_\nu$, where

$$A_\nu = -\frac{\widetilde{\rho}_{11}\omega^2 - Pq_\nu^2}{\widetilde{\rho}_{12}\omega^2 - Qq_\nu^2} = -\frac{\widetilde{\rho}_{12}\omega^2 - Qq_\nu^2}{\widetilde{\rho}_{22}\omega^2 - Rq_\nu^2}, \quad \nu = 1,2. \quad (11)$$

On the other hand, the transverse modes satisfy the equations

$$\mu_b\nabla\times\nabla\times\mathbf{u}_t(\mathbf{r}) - \widetilde{\rho}_{11}\omega^2\mathbf{u}_t(\mathbf{r}) - \widetilde{\rho}_{12}\omega^2\mathbf{U}_t(\mathbf{r}) = 0,$$
$$\widetilde{\rho}_{12}\mathbf{u}_t(\mathbf{r}) + \widetilde{\rho}_{22}\mathbf{U}_t(\mathbf{r}) = 0, \quad (12)$$

which accept plane-wave solutions of the forms $\mathbf{u}_t(\mathbf{r}) = \mathbf{u}_{t0}\exp(i\mathbf{q}_3\cdot\mathbf{r})$ and $\mathbf{U}_t(\mathbf{r}) = \mathbf{U}_{t0}\exp(i\mathbf{q}_3\cdot\mathbf{r})$ with wave number

$$q_3 = \omega\left[\frac{\widetilde{\rho}_{11}}{\mu_b}\left(1 - \frac{\widetilde{\rho}_{12}^2}{\widetilde{\rho}_{11}\widetilde{\rho}_{22}}\right)\right]^{1/2}. \quad (13)$$

As follows directly from the second of Eqs. (12), $\mathbf{U}_t = -(\widetilde{\rho}_{12}/\widetilde{\rho}_{22})\mathbf{u}_t \equiv A_3\mathbf{u}_t$.

The elastic field in a fluid-saturated poroelastic medium at a given frequency can be expanded into longitudinal and transverse vector spherical waves of the appropriate wave number as follows [19,20]:

$$\mathbf{u}(\mathbf{r}) = \sum_{\ell m}\left\{a_{1L\ell m}\frac{1}{q_1}\nabla[j_\ell(q_1r)Y_{\ell m}(\widehat{\mathbf{r}})] + a_{2L\ell m}\frac{1}{q_2}\nabla[j_\ell(q_2r)Y_{\ell m}(\widehat{\mathbf{r}})]\right.$$

$$+ a_{M\ell m} j_\ell(q_3 r)\mathbf{X}_{\ell m}(\hat{\mathbf{r}}) + a_{N\ell m}\frac{i}{q_3}\nabla \times [j_\ell(q_3 r)\mathbf{X}_{\ell m}(\hat{\mathbf{r}})]\Big\}, \quad (14)$$

where j_ℓ are the spherical Bessel functions, which are finite at the origin, $Y_{\ell m}$ are the ordinary spherical harmonics, and $\mathbf{X}_{\ell m}(\hat{\mathbf{r}}) = -i\mathbf{r}\times\nabla Y_{\ell m}(\hat{\mathbf{r}})/\sqrt{\ell(\ell+1)}$ are the vector spherical harmonics ($\mathbf{X}_{00} = 0$). The first term in Eq. (14) describes fast longitudinal waves; the second describes slow longitudinal waves, which are unique to poroelastic media, and the last two terms correspond to transverse waves. A similar expression holds for $\mathbf{U}(\mathbf{r})$ with expansion coefficients $A_1 a_{1L\ell m}$, $A_2 a_{2L\ell m}$, $A_3 a_{M\ell m}$, and $A_3 a_{N\ell m}$ instead of $a_{1L\ell m}$, $a_{2L\ell m}$, $a_{M\ell m}$, and $a_{N\ell m}$, respectively.

In the present paper, we shall consider water-saturated porous silica as the poroelestic material, in which case the values of the relevant parameters are $\rho_s = 2200\,\mathrm{kg\,m^{-3}}$, $c_{sl} = \sqrt{(K_s + 4\mu_s/3)/\rho_s} = 5970\,\mathrm{m\,s^{-1}}$, and $c_{st} = \sqrt{\mu_s/\rho_s} = 3760\,\mathrm{m\,s^{-1}}$ for silica and $\rho_f = 1000\,\mathrm{kg\,m^{-3}}$, $c_f = \sqrt{K_f/\rho_f} = 1480\,\mathrm{m\,s^{-1}}$, and $\eta = 10^{-3}\mathrm{Pa\,s}$ for water. The elastic moduli of the bare skeletal frame, K_b and μ_b, can be experimentally measured independently. However, since there are no experimental data available, following Kargl and Lim [29], we evaluate them using Berryman's self-consistent effective-medium theory for a silica-void elastic composite, assuming that the pores are modeled by randomly distributed needles, which is appropriate for the low-porosity limit that will concern us here [30]. For $f = 10\%$ we find $K_b = 28.9\,\mathrm{GPa}$ and $\mu_b = 23.8\,\mathrm{GPa}$. Accordingly, the tortuosity is given by $\alpha = f^{-2/3}$ for a random array of needles [31].

III. SCATTERING BY A POROELASTIC SPHERE

We now consider a fluid-saturated poroelastic sphere of radius S, centered at the origin of coordinates, immersed in a fluid host medium characterized by mass density ρ_h and bulk modulus K_h. A plane acoustic wave of angular frequency ω incident on that sphere gives rise to a scattered wave, and the total displacement field outside the sphere, expanded into longitudinal spherical waves, has the form [19,20]

$$\mathbf{U}^h(\mathbf{r}) = \sum_{\ell m}\Big\{a^0_{L\ell m}\frac{1}{q_h}\nabla[j_\ell(q_h r)Y_{\ell m}(\hat{\mathbf{r}})] + a^+_{L\ell m}\frac{1}{q_h}\nabla[h^+_\ell(q_h r)Y_{\ell m}(\hat{\mathbf{r}})]\Big\}, \quad (15)$$

where $a^0_{L\ell m}$ and $a^+_{L\ell m}$ are the amplitudes of the spherical-wave components of the incident and scattered fields, respectively, $q_h = \omega\sqrt{\rho_h/K_h}$ is the wave number in the fluid host at the given frequency, and h^+_ℓ are the spherical Hankel functions appropriate for outgoing spherical waves: $h^+_\ell(x) \simeq (-i)^\ell \exp(ix)/(ix)$ as $x\to\infty$. The associated (diagonal) stress tensor

$$\overleftrightarrow{\sigma}^h = \overleftrightarrow{I}\,K_h\nabla\cdot\mathbf{U}^h \equiv -\overleftrightarrow{I}\,p_h \quad (16)$$

defines the pressure p_h in the fluid host.

The expansion coefficients in Eqs. (14) and (15) are determined from those of the incident wave $a^0_{L\ell m}$ uniquely from the following boundary conditions at the surface of the sphere [32]: (a) continuity of the radial, azimuthal, and polar components of the surface traction

$$\overleftrightarrow{\sigma}\hat{\mathbf{r}} = \overleftrightarrow{\sigma}^h\hat{\mathbf{r}}, \quad (17)$$

(b) continuity of the normal component of the filtration velocity

$$f(\dot{U}_r - \dot{u}_r) = \dot{U}^h_r - \dot{u}_r, \quad (18)$$

which ensures conservation of fluid mass, and (c) consistency of the fluid pressure drop and the normal component of the filtration velocity (Darcy's law)

$$f(\dot{U}_r - \dot{u}_r) = -\kappa_s(p_h - p), \quad (19)$$

where κ_s is a parameter that measures interface permeability. For a sealed interface, $\kappa_s = 0$, and for an open interface, $\kappa_s = \infty$.

From the continuity of the radial component of the surface traction we obtain

$$d_{12}a_{1L\ell m} + d_{13}a_{2L\ell m} + d_{14}a_{N\ell m} = b_1 a^0_{L\ell m} - d_{11}a^+_{L\ell m}, \quad (20)$$

where

$$\begin{aligned}
d_{11} &= -x_h h^+_\ell(x_h),\\
d_{12} &= \big\{j_\ell(x_1)\big[x_1^2(\lambda_1+2\mu_b)/K_h - 2\ell(\ell+1)(\mu_b/K_h)\big] + 4x_1 j'_\ell(x_1)(\mu_b/K_h)\big\}\big/x_1,\\
d_{13} &= \big\{j_\ell(x_2)\big[x_2^2(\lambda_2+2\mu_b)/K_h - 2\ell(\ell+1)(\mu_b/K_h)\big] + 4x_2 j'_\ell(x_2)(\mu_b/K_h)\big\}\big/x_2,\\
d_{14} &= 2\sqrt{\ell(\ell+1)}[x_3 j'_\ell(x_3) - j_\ell(x_3)](\mu_b/K_h)/x_3,\\
b_1 &= x_h j_\ell(x_h),
\end{aligned} \quad (21)$$

with $x_\nu = q_\nu S$, $\nu = 1,2,3$, $x_h = q_h S$, and $\lambda_\nu = P - 2\mu_b + Q + A_\nu(Q+R), \nu = 1,2$. Continuity of the tangential components of the surface traction yields

$$[x_3 j'_\ell(x_3) - j_\ell(x_3)]a_{M\ell m} = 0 \quad (22)$$

and

$$d_{22}a_{1L\ell m} + d_{23}a_{2L\ell m} + d_{24}a_{N\ell m} = 0, \quad (23)$$

where

$$\begin{aligned}
d_{22} &= \sqrt{\ell(\ell+1)}[x_1 j'_\ell(x_1) - j_\ell(x_1)]/x_1,\\
d_{23} &= \sqrt{\ell(\ell+1)}[x_2 j'_\ell(x_2) - j_\ell(x_2)]/x_2,\\
d_{24} &= \big\{\big[1 + x_3^2/2 - \ell(\ell+1)\big]j_\ell(x_3) + x_3 j'_\ell(x_3)\big\}\big/x_3.
\end{aligned} \quad (24)$$

From Eq. (18) we obtain

$$d_{32}a_{1L\ell m} + d_{33}a_{2L\ell m} + d_{34}a_{N\ell m} = b_3 a^0_{L\ell m} - d_{31}a^+_{L\ell m}, \quad (25)$$

where

$$\begin{aligned}
d_{31} &= -h^{+\prime}_\ell(x_h),\\
d_{32} &= j'_\ell(x_1)[1 + f(A_1 - 1)],\\
d_{33} &= j'_\ell(x_2)[1 + f(A_2 - 1)],\\
d_{34} &= -\sqrt{\ell(\ell+1)}\,j_\ell(x_3)[1 + f(A_3 - 1)]/x_3,\\
b_3 &= j'_\ell(x_h).
\end{aligned} \quad (26)$$

Finally, Eq. (19), in the case of an open interface ($\kappa_s = \infty \Rightarrow p = p_h$) that will concern us here, gives

$$d_{42}a_{1L\ell m} + d_{43}a_{2L\ell m} = b_4 a^0_{L\ell m} - d_{41}a^+_{L\ell m}, \tag{27}$$

where

$$\begin{aligned} d_{41} &= -x_h h^+_\ell(x_h), \\ d_{42} &= x_1 j_\ell(x_1)[1 - K_b/K_s + f(A_1 - 1)]R/(f^2 K_h), \\ d_{43} &= x_2 j_\ell(x_2)[1 - K_b/K_s + f(A_2 - 1)]R/(f^2 K_h), \\ b_4 &= x_h j_\ell(x_h). \end{aligned} \tag{28}$$

Alternatively, for a finite value of κ_s, from Eq. (19) we obtain

$$d_{42}a_{1L\ell m} + d_{43}a_{2L\ell m} + d_{44}a_{N\ell m} = b_4 a^0_{L\ell m} - d_{41}a^+_{L\ell m}, \tag{29}$$

where

$$\begin{aligned} d_{41} &= \underline{\kappa}_s x_h h^+_\ell(x_h), \\ d_{42} &= i x_h j'_\ell(x_1) f(1 - A_1) - \underline{\kappa}_s x_1 j_\ell(x_1) \\ &\quad \times [1 - K_b/K_s + f(A_1 - 1)]R/(f^2 K_h), \\ d_{43} &= i x_h j'_\ell(x_2) f(1 - A_2) - \underline{\kappa}_s x_2 j_\ell(x_2) \\ &\quad \times [1 - K_b/K_s + f(A_2 - 1)]R/(f^2 K_h), \\ d_{44} &= -i\sqrt{\ell(\ell+1)}\, x_h j_\ell(x_3) f(1 - A_3)/x_3, \\ b_4 &= -\underline{\kappa}_s x_h j_\ell(x_h), \end{aligned} \tag{30}$$

with $\underline{\kappa}_s = \kappa_s\sqrt{K_h \rho_h} = \kappa_s \rho_h c_h$ being a dimensionless interface permeability parameter.

In general, in a linear scattering problem, the partial wave amplitudes of the scattered field and of the field inside the scatterer depend linearly on the corresponding amplitudes of the incident field

$$\begin{aligned} a^+_{P\ell m} &= \sum_{P'\ell'm'} T_{P\ell m;P'\ell'm'} a^0_{P'\ell'm'}, \\ a_{P\ell m} &= \sum_{P'\ell'm'} R_{P\ell m;P'\ell'm'} a^0_{P'\ell'm'}, \end{aligned} \tag{31}$$

where P, P' denote polarization modes. For a spherically symmetric scatterer, the T and R matrices defined through Eq. (31) are diagonal and independent of m. Indeed, as can be readily seen from Eqs. (20), (22), (23), (25), (27), and (29), the matrix elements which are relevant here have the form $T_{L\ell m;L\ell' m'} = T_{LL;\ell}\delta_{\ell\ell'}\delta_{mm'}$ and $R_{P\ell m;L\ell' m'} = R_{PL;\ell}\delta_{\ell\ell'}\delta_{mm'}$. Moreover, Eq. (22), which involves only transverse M modes, is decoupled from the other equations and provides the so-called torsional eigenmodes [33]. These modes are localized in the sphere and cannot be excited by an externally incident acoustic wave. The remaining equations constitute a linear system for the unknowns $T_{LL;\ell}$, $R_{1LL;\ell}$, $R_{2LL;\ell}$, and $R_{NL;\ell}$, which can be written as

$$\begin{pmatrix} d_{11} & d_{12} & d_{13} & d_{14} \\ d_{21} & d_{22} & d_{23} & d_{24} \\ d_{31} & d_{32} & d_{33} & d_{34} \\ d_{41} & d_{42} & d_{43} & d_{44} \end{pmatrix} \begin{pmatrix} T_{LL;\ell} \\ R_{1LL;\ell} \\ R_{2LL;\ell} \\ R_{NL;\ell} \end{pmatrix} = \begin{pmatrix} b_1 \\ b_2 \\ b_3 \\ b_4 \end{pmatrix}, \tag{32}$$

where the various nonzero coefficients are given by Eqs. (21), (24), (26), and (28) or (30). Similar formulas for the scattering T matrix of the submerged fluid-saturated poroelastic sphere have also been reported by others [29,34,35]; however, the explicit expressions derived here correspond to the specific basis of vector spherical waves used in our layer-multiple-scattering method [19,20].

With the help of the T matrix one can directly calculate the change in the number of states of the acoustic field, up to an angular frequency ω, induced by a single poroelastic sphere in an infinite host medium from [36]

$$\Delta N(\omega) = \frac{1}{\pi}\sum_\ell (2\ell + 1)\mathrm{Im}\ln[1 + T_{LL;\ell}(\omega)]. \tag{33}$$

Of more interest is the corresponding change in the density of states induced by the sphere and given by $\Delta n(\omega) = d\Delta N(\omega)/d\omega$. On the other hand, the total scattering and extinction cross sections of the sphere, normalized to the geometric cross section πS^2, can also be expressed in terms of the T matrix as follows [37]:

$$\sigma_{\mathrm{sc}}(\omega) = \frac{4}{x_h^2}\sum_\ell (2\ell + 1)|T_{LL;\ell}(\omega)|^2 \tag{34}$$

and

$$\sigma_{\mathrm{ext}}(\omega) = -\frac{4}{x_h^2}\sum_\ell (2\ell + 1)\mathrm{Re}[T_{LL;\ell}(\omega)], \tag{35}$$

respectively, while the corresponding absorption cross section is given by $\sigma_{\mathrm{abs}} = \sigma_{\mathrm{ext}} - \sigma_{\mathrm{sc}}$.

IV. CLOSE-PACKED PERIODIC STRUCTURES OF SUBMERGED WATER-SATURATED POROUS SILICA SPHERES

We now consider an fcc structure, with lattice constant a, of close-packed porous silica spheres immersed in water and view the crystal structure as a sequence of (111) crystallographic planes. In each plane, the spheres are arranged on a hexagonal lattice with lattice constant $a_0 = a\sqrt{2}/2$, while consecutive planes are separated by a distance $d = a_0\sqrt{6}/3$. We assume that the spheres have a radius $S = a_0/2 = 2.5\,\mu$m. Such mesoporous and macroporous microspheres can be easily synthesized in the laboratory and are promising candidates for diverse applications in many areas ranging from chromatography and catalysis to biology, drug delivery, and medicine [38–46].

We study the acoustic response and phononic eigenmodes of this crystal by means of full elastodynamic calculations using the layer-multiple-scattering method [19,20], which is ideally suited for the case under consideration. Besides the complex phononic band structure of the infinite crystal, the method allows one to calculate also the transmittance $\mathcal{T}$, reflectance $\mathcal{R}$, and absorbance $\mathcal{A} = 1 - \mathcal{T} - \mathcal{R}$ of a finite slab of the crystal at any angle, and in this respect, it can describe an actual acoustic transmission experiment. Another advantage of the method is that it solves the elastodynamic equations in the frequency domain and, therefore, it can treat dispersion and viscous losses, which naturally occur in poroelastic materials, in a straightforward manner. The properties of the individual scatterers enter only through the corresponding T matrix. In the first step, in-plane multiple scattering is evaluated in the spherical-wave basis, introduced in the previous section, using proper propagator functions.

Subsequently, interlayer scattering is calculated in a plane-wave basis through appropriate transmission and reflection matrices by including all propagating and evanescent components of the wave field necessary to obtain convergence. Therefore, interaction between the scatterers is fully taken into account. The scattering S matrix of a multilayer slab, which transforms the incoming into the outgoing wave field, is obtained by combining the transmission and reflection matrices of the component layers. The ratio of the transmitted or reflected energy flux to the energy flux associated with the incident wave defines the transmittance or reflectance of the slab, respectively, while the absorbance is deduced from the requirement of energy conservation. On the other hand, for a three-dimensional crystal consisting of an infinite periodic sequence of layers, stacked along the z direction, applying the Bloch condition for the wave field in the region between two consecutive unit slabs leads to an eigenvalue equation, which gives the z component of the Bloch wave vector k_z, for the given angular frequency ω and in-plane wave-vector component reduced within the surface Brillouin zone $\mathbf{k}_\parallel$, which are conserved quantities in the scattering process as a result of time and two-dimensional translation invariance, respectively. The eigenvalues $k_z(\omega,\mathbf{k}_\parallel)$, looked upon as functions of real ω, define, for each $\mathbf{k}_\parallel$, lines in the complex k_z plane. Taken together, they constitute the complex band structure of the infinite crystal associated with the given crystallographic plane. A line of given $\mathbf{k}_\parallel$ may be real (in the sense that k_z is real) over certain frequency regions and may be complex (in the sense that k_z is complex) for ω outside these regions. It turns out that, for given ω and $\mathbf{k}_\parallel$, out of the eigenvalues $k_z(\omega,\mathbf{k}_\parallel)$ none or, at best, a few of them are real, and the corresponding eigenvectors represent propagating modes of the acoustic field in the given infinite crystal. The remaining eigenvalues $k_z(\omega,\mathbf{k}_\parallel)$ are complex, and the corresponding eigenvectors represent evanescent waves. These have an amplitude that increases exponentially in the positive or negative z direction and, unlike the propagating waves, do not exist as physical entities in the infinite crystal. However, they are an essential part of the physical solutions of the acoustic field in a slab of finite thickness. A region of frequency where propagating waves do not exist, for given $\mathbf{k}_\parallel$, constitutes a frequency gap of the acoustic field for this $\mathbf{k}_\parallel$. If over a frequency region no propagating wave exists whatever the value of $\mathbf{k}_\parallel$, then this region constitutes an absolute frequency gap. In order to ensure good convergence in our calculations, it is sufficient to truncate the spherical-wave expansions at $\ell_{\max} = 8$ and take into account 37 two-dimensional reciprocal lattice vectors in the relevant plane-wave expansions [20] in all cases we examine here.

In Fig. 1, we display the calculated transmission and absorption spectra of an eight-layer-thick (111) slab of the crystal under consideration at normal incidence for given porosity $f = 10\%$ but different pore sizes. In the small-pore-size limit with respect to the viscous skin depth $\delta = \sqrt{2\eta/(\omega\rho_f)}$ [see Fig. 1(a)], within the considered range of frequencies, Poiseuille flow occurs. Locking of fluid and solid motion arises from the fluid viscosity and results in propagation of a fast wave, while the out-of-phase relative motion of the solid frame and infiltrated liquid, required for slow wave propagation, cannot be efficiently realized. In this regime, the porous material behaves as a homogeneous medium with effective elastic parameters that can be calculated using the self-consistent effective-medium theory of Berryman for elastic composites [30]. Nevertheless, also in this case, the absorptive losses are associated with the slow wave modes and cannot be accounted for by effective-medium theory, even retaining the energy dissipation mechanism by attributing a shear modulus $\mu_f = -i\omega\eta$ to the fluid component. Since there is no significant difference in the final results of the effective-medium calculations with and without losses in the frequency range studied, we neglect for convenience the viscosity of water, so all effective material parameters are dispersionless and real valued. We obtain $\overline{\rho} = 2080\,\mathrm{kg\,m^{-3}}$, $\overline{c_l} = 5449\,\mathrm{m\,s^{-1}}$, and $\overline{c_t} = 3389\,\mathrm{m\,s^{-1}}$. It is interesting to note that frictional dissipation due to the slow waves is in this case much larger than in the corresponding single sphere (σ_{abs} is very small) due to multiple-scattering effects. As the pore size increases, the out-of-phase relative motion of the solid and fluid is not impeded by viscous drag, so the slow wave can propagate, giving rise to enhanced absorptive losses and a consequent drastic drop in the transmittance [see Figs. 1(b) and 1(c)]. On the other hand, for very large pores, if the viscous skin depth is negligible with respect to the pore size, the three density parameters in Eqs. (10) and (13) become real, and all three bulk modes become nondispersive and attenuation free, as one would have in the absence of viscous losses ($\eta = 0$). This trend can be clearly seen in Fig. 1(d). In this regime Poiseuille flow is not established, and fast wave propagation is driven by inertial coupling, which locks the solid and fluid components together. It becomes clear from the above that porous silica nanoparticles, immersed

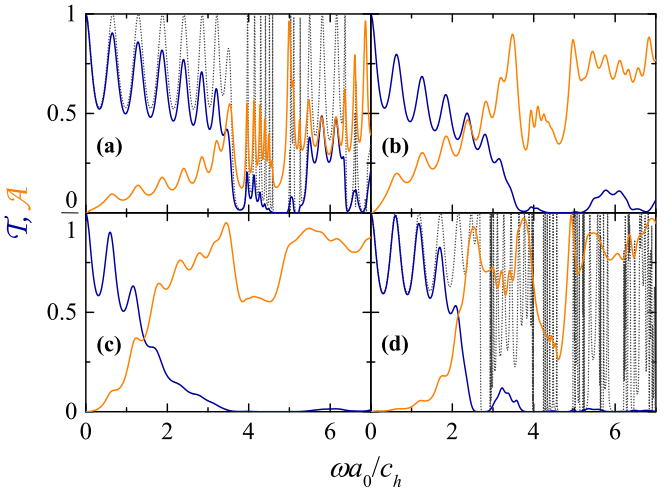

FIG. 1. Transmittance and absorbance of an acoustic plane wave incident normally on a slab consisting of eight fcc (111) planes of submerged water-saturated close-packed porous silica spheres of radius $S = 2.5$ μm, with porosity $f = 10\%$, for different pore sizes: (a) $R_p = 10$ nm, (b) $R_p = 30$ nm, (c) $R_p = 100$ nm, and (d) $R_p = 500$ nm. The dotted lines in (a) and (d) display the corresponding transmission spectra for crystals made of homogeneous spheres with elastic parameters calculated using self-consistent effective-medium theory for (lossless) composite elastic media [30] and of water-saturated porous spheres neglecting viscous losses ($\eta = 0$), respectively.

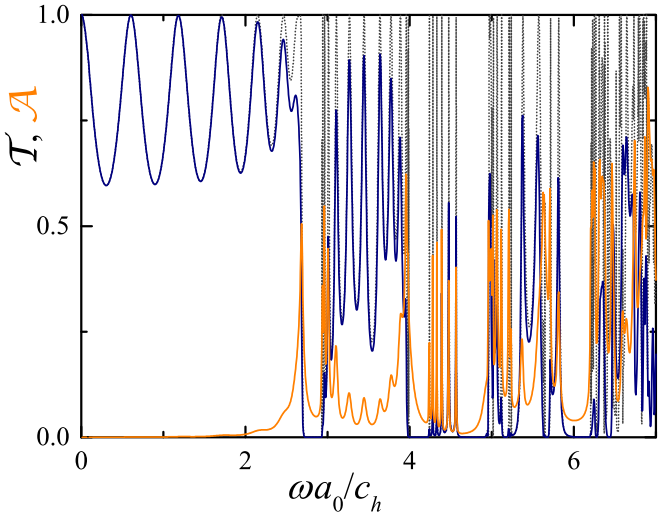

FIG. 2. The same as in Fig. 1(d) for spheres of porosity $f = 10\%$ but radius $S = 2.5$ mm and pore radius $R_p = 500\,\mu$m.

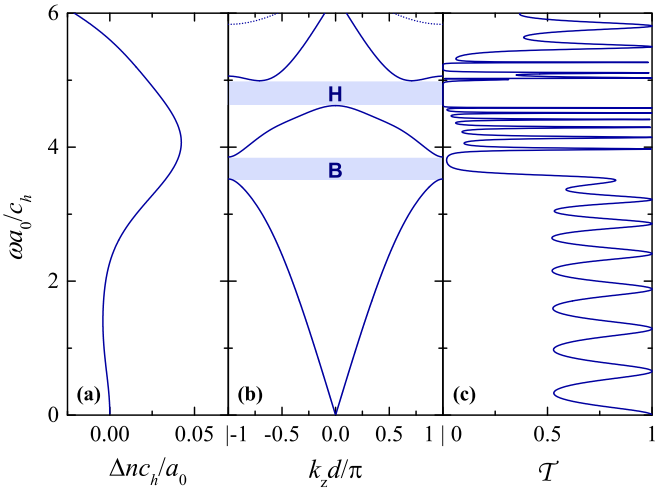

FIG. 3. (a) Change in the density of states of the acoustic field induced by a submerged water-saturated porous silica sphere with porosity $f = 10\%$, treated as a lossless homogeneous sphere with elastic parameters calculated using self-consistent effective-medium theory for composite elastic media [30]. (b) The phononic band structure of an fcc crystal of such close-packed homogeneous spheres, in water, along the [111] direction. Solid (dotted) lines refer to nondegenerate (doubly degenerate) bands of Λ_1 (Λ_3) symmetry. The shaded areas mark the Bragg (B) and hybridization (H) gaps. (c) Transmittance of an acoustic plane wave incident normally on a (111) slab of this crystal, eight layers thick.

in a waterlike liquid, at hypersonic (gigahertz) frequencies are in the viscous coupling regime. This explains why, treating such particles as effectively homogeneous with elastic parameters smaller than those of pure solid silica, one can successfully explain Brillouin light-scattering experiments on corresponding colloidal crystals [14].

We can approach more closely the inertial coupling limit if we increase all characteristic length parameters of the system by a factor of ξ, i.e., $R_p \to \xi R_p$, $S \to \xi S$, $a \to \xi a$, in which case the viscous-length-to-porous-size ratio decreases by a factor of $\sqrt{\xi}$ ($\frac{\delta}{R_p} \to \frac{1}{\sqrt{\xi}}\frac{\delta}{R_p}$) in the same region of reduced frequency $\omega a_0/c_h$. For example, it can be seen in Fig. 2 that for submerged water-saturated close-packed porous silica spheres of radius $S = 2.5$ mm, porosity $f = 10\%$, and pore radius $R_p = 500\,\mu$m, the transmission spectrum is very similar to that of the corresponding lossless case ($\eta = 0$), while the absorbance is overall strongly suppressed and exhibits sharp peaks only at the resonances where the wave field is predominantly localized at the spheres.

The transmission spectra of the reference lossless structures in the viscous and inertial coupling regimes, shown by dotted lines in Figs. 1(a) and 1(d) and replotted in Figs. 3(c) and 4(c), can be interpreted in conjunction with relevant dispersion diagrams for the corresponding infinite crystals, depicted in Figs. 3(b) and 4(b), respectively. It can be seen that the transmittance exhibits Fabry-Pérot oscillations in regions of acoustically active bands due to multiple reflections at the surfaces of the slab and drops down to small values outside these regions. The phononic band structure of these crystals can be understood as follows. An extended acoustic band, which would be in a corresponding effective homogeneous medium, is folded within the first Brillouin zone as a result of structure periodicity, and Bragg gaps open up at the zone boundaries. In addition, there are narrow bands originating from localized modes of the individual spheres, weakly interacting between them. These modes are manifested as resonance peaks in the corresponding density of states, as shown in Figs. 3(a) and 4(a). When bands of the same symmetry cross each other, a band gap, the so-called hybridization gap, opens up about the crossing point due to level repulsion. The bands along the fcc [111] direction have the symmetry of the irreducible representations of the C_{3v} point group [47]. Therefore, they are either nondegenerate if they have the Λ_1 or the Λ_2 symmetry or doubly degenerate if they have the Λ_3 symmetry. Only the Λ_1 bands are acoustically active in the sense that they can be excited by an acoustic plane wave with appropriate

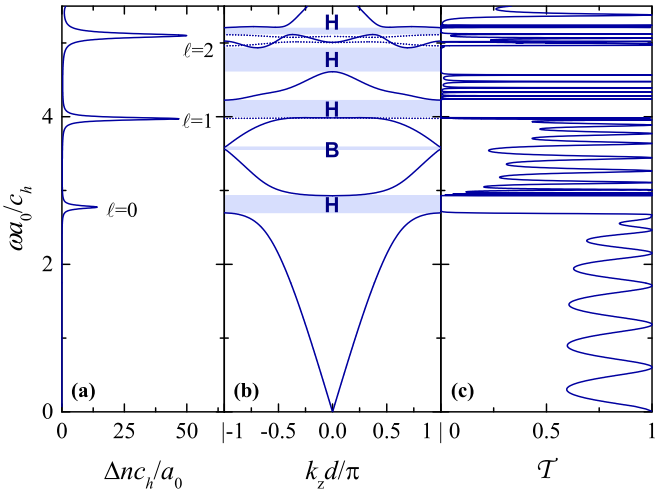

FIG. 4. The same as Fig. 3 but for submerged water-saturated porous silica spheres described by Biot's theory, ignoring viscous losses ($\eta = 0$). The peaks in (a) correspond to resonances of given multipole order ℓ denoted in the diagram.

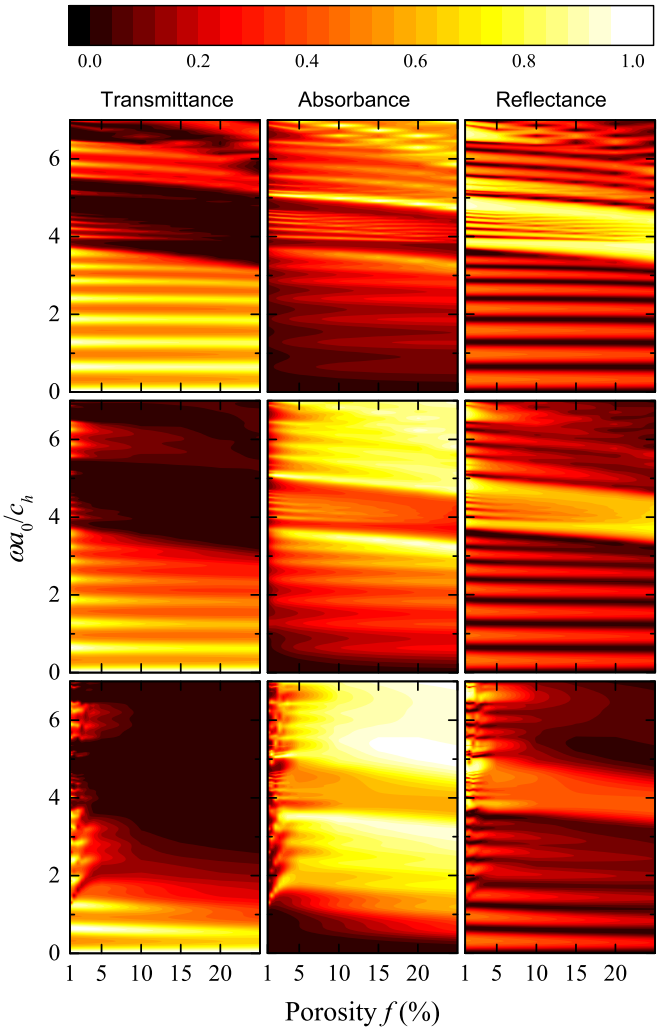

FIG. 5. Transmittance, absorbance, and reflectance of an acoustic plane wave incident normally on a slab consisting of eight fcc (111) planes of submerged water-saturated close-packed porous silica spheres of radius $S = 2.5\,\mu$m versus the porosity f for different pore sizes. Pore radius (from top to bottom): $R_p = 10$, 30, and 100 nm.

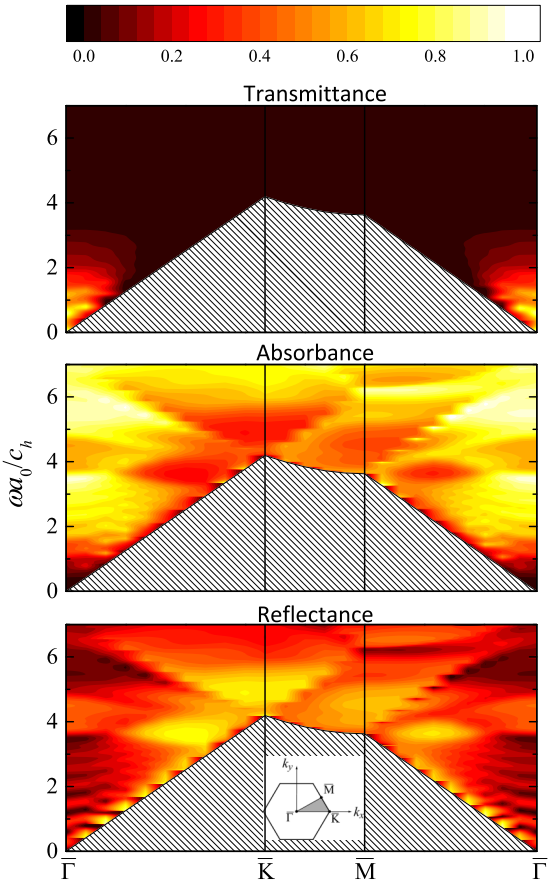

FIG. 6. Transmittance, absorbance, and reflectance of an acoustic plane wave incident on a slab consisting of eight fcc (111) planes of submerged water-saturated close-packed porous silica spheres ($S = 2.5\,\mu$m, $f = 10\%$, and $R_p = 100$ nm) with $\mathbf{k}_\parallel$ along high-symmetry lines of the fcc (111) surface Brillouin zone, shown in the inset. $\overline{\Gamma}$: $\mathbf{k}_\parallel = \frac{2\pi}{a_0}(0,0)$, $\overline{\mathrm{K}}$: $\mathbf{k}_\parallel = \frac{2\pi}{a_0}(\frac{2}{3},0)$, $\overline{\mathrm{M}}$: $\mathbf{k}_\parallel = \frac{2\pi}{a_0}(\frac{1}{2},\frac{\sqrt{3}}{6})$.

frequency incident normally on a (111) slab of the crystal because they have the proper symmetry [48]. It is expected that strong absorption will appear in band regions with a large admixture of modes localized in and about the spheres when the dissipation mechanism triggered by the slow waves in the porous material is switched on. It can be seen that this is the case, for example, in the flat band regions originating from the multipole resonances of the spheres (see Fig. 4), where high absorption is attained, as shown in Fig. 1(d).

The above porous-based phononic crystal exhibits interesting absorptive properties and can be used as an efficient filter through an appropriate selection not only of the pore size but also of the porosity level. In Fig. 5 we show the transmittance, absorbance, and reflectance of an acoustic plane wave incident normally on a slab of this crystal, consisting of eight fcc (111) layers, for different pore sizes R_p as a function of the porosity f. Broadband high-level absorbance can be attained for rather intermediate R_p/δ ($R_p = 100$ nm) and relatively low porosity values, varying from $f = 10\%$ to 25%. The porosity f, as an additional degree of freedom, can be chosen to achieve for rather moderate R_p/δ the appearance of regions of frequency where both the transmittance and reflectance practically vanish, leading to $\mathcal{A} \simeq 1$.

It is interesting to note that broadband acoustic isolation occurs for waves not only incident normally but also at an angle on a slab of the material. This is shown in Fig. 6, which displays the variation of the transmission spectra of an eight-layer-thick fcc (111) slab of submerged water-saturated close-packed porous silica spheres, with $S = 2.5\,\mu$m, $f = 10\%$, and $R_p = 100$ nm for different $\mathbf{k}_\parallel$ along high symmetry lines of the fcc (111) surface Brillouin zone. The direction of incidence is specified by the corresponding polar and azimuthal angles, $\theta = \arccos(\sqrt{1 - c_h^2 k_\parallel^2/\omega^2})$ and $\phi = \arctan(k_y/k_x)$, respectively. Obviously, at given $\mathbf{k}_\parallel$, propagating incident waves exist above an angular frequency threshold $\omega_{\mathrm{inf}} = c_h|\mathbf{k}_\parallel|$ (delimiting the hatched area in Fig. 6). It can be seen (and we verified it for other arbitrary points $\mathbf{k}_\parallel$ within the surface Brillouin zone as well) that, above $\omega a_0/c_h \simeq 2$, the transmittance practically vanishes, whatever the direction of incidence.

V. CONCLUSIONS

In summary, we generalized the layer-multiple-scattering method to phononic crystals of poroelastic spheres immersed in a fluid medium and presented specific applications of the method to close-packed fcc crystals of submerged water-saturated meso- and macroporous silica microspheres, encompassing the viscous and inertial coupling regimes. It is worth noting that the formalism presented in the present paper remains invariant under a transformation $\omega \to \xi\omega$ and $R_p \to R_p/\xi$, $S \to S/\xi$, $a \to a/\xi$, $\eta \to \eta/\xi$, where ξ is an arbitrary constant factor. Therefore, our results apply to different regions of frequency of the acoustic field, provided that all size parameters as well as the viscosity coefficient are scaled accordingly. Our results are analyzed by reference to phononic dispersion diagrams, which are appropriate for the viscous and inertial coupling limits, in conjunction with corresponding transmission spectra, providing a consistent interpretation of the underlying physics. For intermediate pore sizes, it is shown that, with increasing porosity, strong absorption leads to negligible transmission over an extended frequency range, which might be useful for broadband acoustic shielding applications. Our work paves the way towards a new class of phononic structures that exhibit unprecedented properties driven by the slow longitudinal waves, which are unique to poroelastic materials, and multiple-scattering effects. These structures cannot be described by treating the poroelastic material as an effective homogeneous medium, and rigorous methods based on Biot's theory, such as that developed in the present paper, are required.

ACKNOWLEDGMENTS

A.A. was supported by the project SUPERMEN through a postgraduate fellowship. This project is cofinanced by the European Union through the European Regional Development Fund and by the Conseil Regional de Haute Normandie.

[1] *Acoustic Metamaterials and Phononic Crystals*, edited by P. A. Deymier, Springer Series in Solid-State Sciences Vol. 173 (Springer, Berlin, 2013).
[2] *Phononic Crystals: Fundamentals and Applications*, edited by A. Khelif and A. Adibi (Springer, New York, 2016).
[3] M. Sigalas and E. N. Economou, J. Sound Vib. **158**, 377 (1992).
[4] M. S. Kushwaha, P. Halevi, L. Dobrzynski, and B. Djafari-Rouhani, Phys. Rev. Lett. **71**, 2022 (1993).
[5] Z. Y. Liu, X. X. Zhang, Y. W. Mao, Y. Y. Zhu, Z. Y. Yang, C. T. Chan, and P. Sheng, Science **289**, 1734 (2000).
[6] B. Rostami-Dogolsara, M. K. Moravvej-Farshi, and F. Nazari, Phys. Rev. B **93**, 014304 (2016).
[7] A. Khelif, B. Djafari-Rouhani, J. O. Vasseur, P. A. Deymier, Ph. Lambin, and L. Dobrzynski, Phys. Rev. B **65**, 174308 (2002).
[8] J. H. Sun and T. T. Wu, Phys. Rev. B **71**, 174303 (2005).
[9] F. L. Hsiao, A. Khelif, H. Moubchir, A. Choujaa, C. C. Chen, and V. Laude, Phys. Rev. E **76**, 056601 (2007).
[10] S. Amoudache, R. Moiseyenko, Y. Pennec, B. Djafari-Rouhani, A. Khater, R. Lucklum, and R. Tigrine, J. Appl. Phys. **119**, 114502 (2016).
[11] S. Yang, J. H. Page, Z. Y. Liu, M. L. Cowan, C. T. Chan, and P. Sheng, Phys. Rev. Lett. **93**, 024301 (2004).
[12] H. S. Lim, M. H. Kuok, S. C. Ng, and Z. K. Wang, Appl. Phys. Lett. **84**, 4182 (2004).
[13] T. Still, R. Sainidou, M. Retsch, U. Jonas, P. Spahn, G. P. Hellmann, and G. Fytas, Nano Lett. **8**, 3194 (2008).
[14] T. Still, G. Gantzounis, D. Kiefer, G. Hellmann, R. Sainidou, G. Fytas, and N. Stefanou, Phys. Rev. Lett. **106**, 175505 (2011).
[15] *Porous Media Applications in Biological Systems and Biotechnology*, edited by K. Vafai (CRC Press, Boca Raton, FL, 2010).
[16] *Porous Materials: Processing and Applications*, edited by P. S. Liu and G. F. Chen (Elsevier, Amsterdam, 2014).
[17] *Handbook of Porous Media*, edited by K. Vafai (CRC Press, Boca Raton, FL, 2015).
[18] W. Trabelsi, H. Franklin, A. Tinel, and S. Derible, Ultrasonics **54**, 1097 (2014).
[19] I. E. Psarobas, N. Stefanou, and A. Modinos, Phys. Rev. B **62**, 278 (2000).
[20] R. Sainidou, N. Stefanou, I. E. Psarobas, and A. Modinos, Comput. Phys. Commun. **166**, 197 (2005).
[21] M. A. Biot, J. Acoust. Soc. Am. **28**, 168 (1956).
[22] M. A. Biot, J. Acoust. Soc. Am. **28**, 179 (1956).
[23] M. A. Biot, J. Acoust. Soc. Am. **34**, 1254 (1962).
[24] M. A. Biot, J. Appl. Phys. **33**, 1482 (1962).
[25] R. D. Stoll and G. M. Bryan, J. Acoust. Soc. Am. **47**, 1440 (1970).
[26] J. G. Berryman, Appl. Phys. Lett. **37**, 382 (1980).
[27] *Handbook of Mathematical Functions*, edited by M. Abramowitz and I. A. Stegun (Dover, New York, 1965).
[28] D. L. Johnson, J. Koplik, and R. Dashen, J. Fluid Mech. **176**, 379 (1987).
[29] S. G. Kargl and R. Lim, J. Acoust. Soc. Am. **94**, 1527 (1993).
[30] J. G. Berryman, J. Acoust. Soc. Am. **68**, 1809 (1980); **68**, 1820 (1980).
[31] P. N. Sen, C. Scala, and M. H. Cohen, Geophysics **46**, 781 (1981).
[32] H. Deresiewicz and R. Skalak, B. Seismol. Soc. Am. **53**, 783 (1963).
[33] H. Lamb, Proc. London Math. Soc. **s1-13**, 189 (1882).
[34] S. M. Hasheminejad and S. A. Badsar, Q. J. Mech. Appl. Math. **57**, 95 (2004).
[35] S. M. Hasheminejad and S. A. Badsar, Jpn. J. Appl. Phys. **43**, 2612 (2004).
[36] R. Sainidou, N. Stefanou, and A. Modinos, Phys. Rev. B **69**, 064301 (2004).
[37] I. E. Psarobas, Phys. Rev. B **64**, 012303 (2001).
[38] J. J. Kirkland, J. Chromatogr. **125**, 231 (1976).
[39] Z. G. Shi and Y. Q. Feng, Microporous Mesoporous Mater. **116**, 701 (2008).
[40] L. H. Chen, G. S. Zhu, D. L. Zhang, H. Zhao, M. Y. Guo, W. Shi, and S. L. Qiu, J. Mater. Chem. **19**, 2013 (2009).
[41] Z. G. Shi, Q. Z. Guo, Y. T. Liu, Y. X. Xiao, and L. Xu, Mater. Chem. Phys. **126**, 826 (2011).

[42] Y. S. Cho, S. Y. Choi, Y. K. Kim, and G. R. Yi, J. Colloid. Interf. Sci. **386**, 88 (2012).
[43] J. He, C. L. Yang, X. H. Xiong, and B. W. Jiang, J. Polym. Sci., Part A **50**, 2889 (2012).
[44] C. Cheng, T. Z. Yang, Y. H. He, L. Yang, and L. X. Wang, Mater. Lett. **109**, 257 (2013).
[45] S. Grama and D. Horák, Physiol. Res. **64**(Supl. 1), S11 (2015).
[46] H. J. Xia, G. P. Wan, F. Yang, J. S. Wang, and Q. Bai, Mater. Lett. **180**, 19 (2016).
[47] J. F. Cornwell, *Group Theory and Electronic Energy Bands in Solids* (North-Holland, Amsterdam, 1969).
[48] I. E. Psarobas, A. Modinos, R. Sainidou, and N. Stefanou, Phys. Rev. B **65**, 064307 (2002).